Journal of Imaging Science and Technology® 51(5): 391–401, 2007.

Digital Color Image Halftone: Hybrid Error Diffusion Using the Mask Perturbation and Quality Verification

JunHak Lee, Takahiko Horiuchi, Ryoichi Saito and Hiroaki Kotera
Graduate School of Science and Technology, Chiba University, 1-33, Yayoi-cho, Inage-ku, Chiba-Shi, Chiba, 263-8522, Japan
E-mail: leejunhak@graduate.chiba-u.jp

Abstract. *Error diffusion is widely used in digital image halftones. The algorithm is very simple to implement and very fast to calculate. However, it is known that standard error diffusion algorithms, such as the Floyd Steinberg error diffusion, produce undesirable artifacts in the form of structure artifacts, such as worms, checkerboard patterns, diagonal stripes, and other repetitive structures. The boundaries between structural artifacts break the visual continuity in regions of low intensity gradients and therefore may be responsible for false contours. In this paper, we propose a new halftone method to reduce the structural artifacts and to improve the gray expression, called hybrid error diffusion, by using the concept of "error diffusion by perturbing the error coefficient with a mask." The proposed algorithm consists of two steps in each pixel position. In the first step, a perturbation is calculated using the internal pseudorandom number and a selected* 4×4 *mask, similar to a dither mask. In the second step, error diffusion weights are calculated with the criterion for each pixel value. The proposed hybrid method can reduce the structural artifacts while keeping the advantage of the error diffusion. This paper discusses the performance of the proposed algorithm with experimental results for natural test images. Then, objective assessment results are given using statistical tools and the structural similarity measure for color images.*
[DOI: 10.2352/J.ImagingSci.Technol.(2007)51:5(391)]

INTRODUCTION

Halftoning is a method of producing the pseudocontinuous tone images using only a finite number of gray levels. Because of the inherent characteristic of the human visual system with regard to observing average gray level over an area, the human observer perceives intermediate tones. Generally, halftoning is considered as a simple "on" and "off" modulation technique, where the sensation of intermediate tones is created by the presence and absence of a pixel. The digital halftone technology plays an important role in transforming a continuous tone (gray or color) image to an image with a reduced number of gray levels for display devices.

For halftone technologies, each pixel value is determined to be white or black when compared to the threshold value, and the quantization error is then fed back and added to adjacent pixels.[1,2] The conventional error diffusion algorithm has the advantages of simple implementation and fast calculation speed. It uses the concept of overflow and diffusion of the quantized error, and then resets the diffusion. However, the conventional error diffusion algorithm introduces distortion, reducing the visibility, worms, and false textures or additive noise. In order to solve these problems, many digital halftone algorithms have been proposed. Examples include using variable thresholds,[3] and variable filter weights[4–6] with input data. There were also approaches that considered the color channel correlation[6–8] for improving the color halftone visibility in color images. However, these methods require a complex process and long calculation time or many lookup tables.

In this paper, we propose a well-organized halftone algorithm, hybrid error diffusion (HED) to improve the conventional halftone artifacts and enhance the visibility of color. The proposed algorithm is very simple, easy to implement, and can reduce the structural artifacts, keeping with the advantage of the error diffusion algorithms. We use the concept of a perturbing error filter weight by using the mask value, which is perturbed with a pseudorandom number. The proposed algorithm is basically the same as using the four-tap style error filter similar to that of the Floyd–Steinberg error diffusion. The basic procedure of the proposed algorithm is as follows:

1. Determine the mask value for each color plane and added to pseudorandom number.
2. Calculate the error filter weights for each color plane.

The mask that is used is similar to the ordered dither mask. The mask value is selected by pixel, line, and each color plane. We also use the different error filter weights for each color plane to enhance the color visibility. The error filter weights were calculated by using a different mask for each color plane. The results of the proposed algorithm show good performance for reducing artifacts, worms, and false textures.

The paper is organized as follows. In the next section, we review the conventional error diffusion algorithm and investigate its general problem. In the Hybrid Error Diffusion Algorithm section, we explain the proposed HED algorithm in detail. In Experimental Results, we introduce the conventional halftone evaluation tools, pair correlation, and radially averaged power spectrum density. As another method of halftone evaluation, a structural similarity mea-

Received Oct. 28, 2006; accepted for publication Jun. 5, 2007.
1062-3701/2007/51(5)/391/11/$20.00.

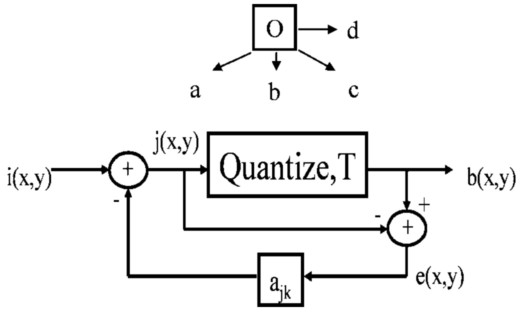

Figure 1. General block diagram of conventional error diffusion.

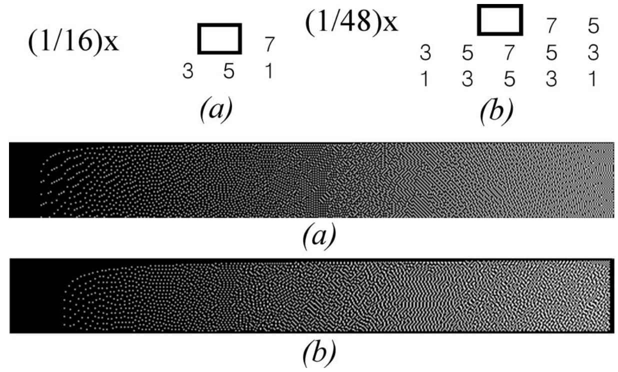

Figure 2. Simulation results of conventional error diffusion algorithm.

sure between color images is also derived. Then, the simulation results of the algorithms are given with natural images. We also compare our algorithm with conventional methods using the objective assessment, halftone statistical analysis, and color image structural similarity measure. Finally, there is the Conclusion.

CONVENTIONAL ERROR DIFFUSION ALGORITHM

There are many error diffusion algorithms for improving the halftone quality.[1–12] Almost of the conventional algorithms are designed based on the Floyd–Steinberg error diffusion algorithm. In this section, we investigate the Floyd–Steinberg algorithm[1] and the Jarvice et al.[2] error diffusion algorithm, as a representative conventional error diffusion algorithm, to simulation results. In Figure 1, each signal can be defined as follows:

$$b(x,y) = \begin{cases} 1, & \text{if} \quad j(x,y) \geq T, \\ 0, & \text{otherwise,} \end{cases} \tag{1}$$

$$j(x,y) = i(x,y) - \sum (a_{jk} e(x-j, y-k)), \tag{2}$$

$$e(x,y) = b(x,y) - j(x,y), \tag{3}$$

where $i(x,y)$ is the input image and the $b(x,y)$ is the output image of the halftone process. The signal $j(x,y)$ represents the modified input, a_{jk} are the error filter weights, $\Sigma a_{jk}=1$, and T is the threshold value. The signal $e(x,y)$ is the accumulated error value that will be diffused to adjacent pixels. The conventional error diffusion algorithm has the advantage of simple implementation and fast calculation. However, the conventional error diffusion introduces the distortion that reduces image quality and produces worms, false textures, and additive noise. The simulation results of the Floyd–Steinberg error diffusion algorithm and the Jarvice et al.[2] error diffusion algorithm are given in Figure 2. The input image is the "gradation ramp" of increasing gray levels from 0 to 128 gray levels with the slope of 4 pixels per gray level. From the simulation results, we can see the prominent discontinuity and a white dot in the middle of the gradation. In the low gray area, we can also see diagonal stripes. The worm patterns are also in the middle of the gradation ramp. The reduction of these kinds of conventional artifacts is the objective of the proposed algorithm. At the end of this paper, we compare the results of conventional error diffusion to the results of the Floyd–Steinberg error diffusion, vector color error diffusion,[7] and Shiau–Fan error diffusion[10] with natural images.

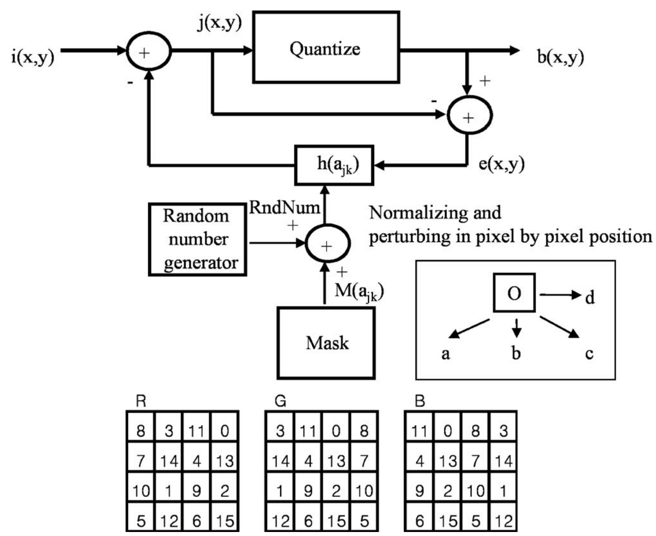

Figure 3. Block diagram of hybrid error diffusion.

HYBRID ERROR DIFFUSION ALGORITHM

We use the concept of perturbing error filter weight by using the mask value, which is perturbed with a pseudorandom number. The concept of the proposed hybrid error diffusion is shown in Figure 3, in which each signal can be defined as follows:

$$b(x,y) = \begin{cases} 1, & \text{if} \quad j(x,y) \geq T \\ 0, & \text{otherwise,} \end{cases} \tag{4}$$

$$j(x,y) = i(x,y) - \sum (h(a_{jk}) e(x-j, y-k)), \tag{5}$$

$$e(x,y) = b(x,y) - j(x,y), \tag{6}$$

$$M(a_{jk}) = \text{MaskValue}|_{\text{for each color/line/pixel}}, \tag{7}$$

$$h(a_{jk}) = (\text{RndNum} + M(a_{jk})), \tag{8}$$

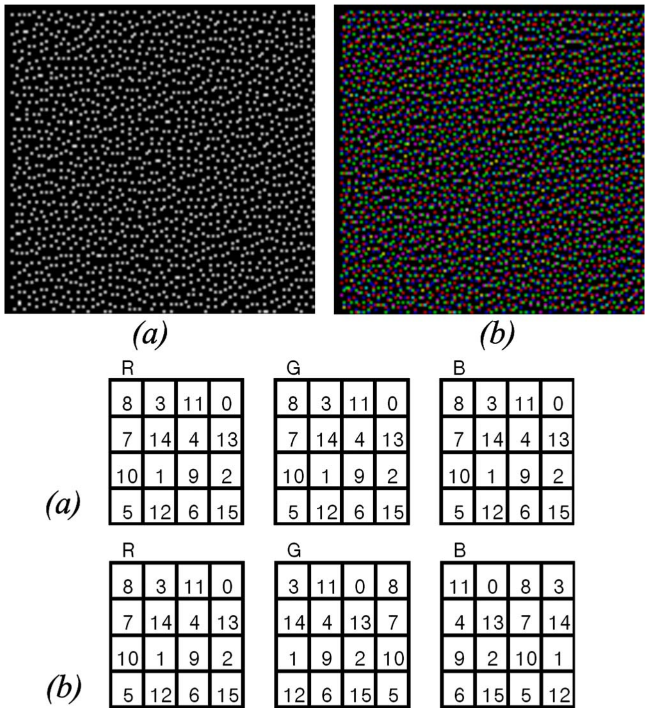

Figure 4. Results of gray level 28: (a) R, G, B same mask and (b) R, G, B different mask.

$$\sum h(a_{jk}) = 1, \quad h(a_{jk}) \geq 0, \tag{9}$$

where $i(x,y)$ is the input image and $b(x,y)$ is the output image of the halftone process. $j(x,y)$ represents the modified input, and $e(x,y)$ is the accumulated error value that will be diffused to adjacent pixels. $M(a_{jk})$ is the selected mask value, which is dependent on the pixel position and color plane. $h(a_{jk})$ are the error filter weights, and T is the threshold value. The four-tap style error filter weight of the proposed algorithm is similar to that of the Floyd–Steinberg error diffusion algorithm. However, the internal pseudorandom number generator and mask selector is newly added to that. The error filter weights $h(a_{jk})$ are varied with the internally calculated pseudorandom number and the mask value. The mask that is used is similar to the ordered dither mask. This mask value is selected by pixel, line, and color plane. As a result, the error filter weight varies with the pixel position, line, and color plane. Finally, the error filter weight $h(a_{jk})$ values are determined pixel by pixel by the criterion of Eq. (9).

The procedure of calculating the error carry is as follows. First, the mask value is determined based on the color plane, the pixel position, and the line position. For example, if the color plane is red (R), the (pixel, line)=(3, 3), the mask value will be 9 in the R of Fig. 3. Next, a pseudorandom number is added to the predetermined mask value. Finally, the error filter weights are determined by a normalizing process for each pixel and color plane. Then, the diffusion process is carried out, which is similar to conventional error diffusion. In view of hardware implementation, for example, the mask values and pseudorandom number seeds can already be stored in the internal RAM (random access memory) area. The generation and reading process can be carried out in pixel calculation duration.

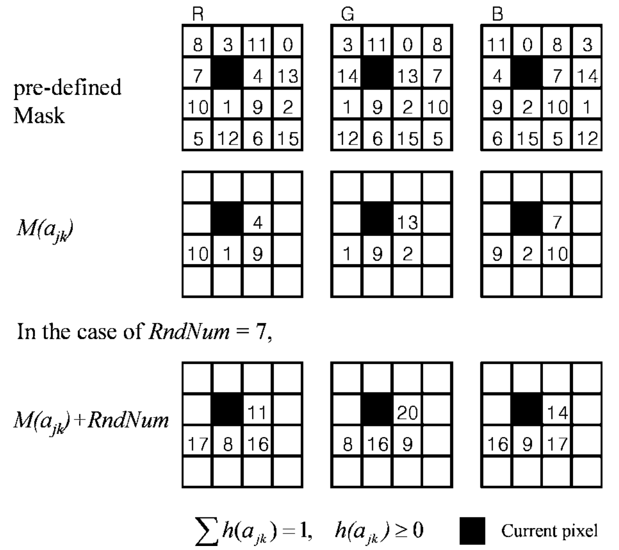

Figure 5. Determination of the error weight $h(a_{jk})$.

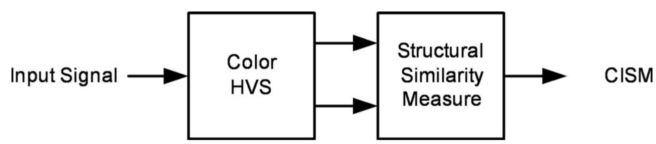

Figure 6. System block diagram for CISM.

We use a different mask for each color plane to improve the color visibility. The results are compared in Figure 4. The result of (a) comes from using the same R, G, and B masks, while the result of (b) is from using different R, G, and B masks as shown. We can see that the white dots in the result of (a) are replaced by the mixing of R, G, and B dots in the case of (b). We can confirm the increasing effect of halftone carry density in these results. The green (G) and blue (B) masks are generated from the red mask. The red mask is generated with the relation of check board weight. That is, the green mask is generated by moving 1 pixel to left of the red mask. The blue mask is generated by moving 2 pixels to left of the red mask. In Figure 5, the example is given in the case of the RndNum=7 for each color plane.

It is possible to control the error diffusion pattern by controlling the mask value. Because the error diffusion pattern mainly depends on the error filter shape, the scan direction, and error filter weights, we can control the error diffusion pattern by controlling the R, G, and B masks.

EXPERIMENTAL RESULTS

Introduction to Halftone Evaluation

In this section, we introduce assessment tools used to evaluate the HED algorithm. In order to evaluate the halftone, we use conventional halftone statistics. However, it is difficult to verify the similarity of the structural pattern using conventional verification measures. In this paper, we use the color image similarity measure for evaluating the structural pattern.

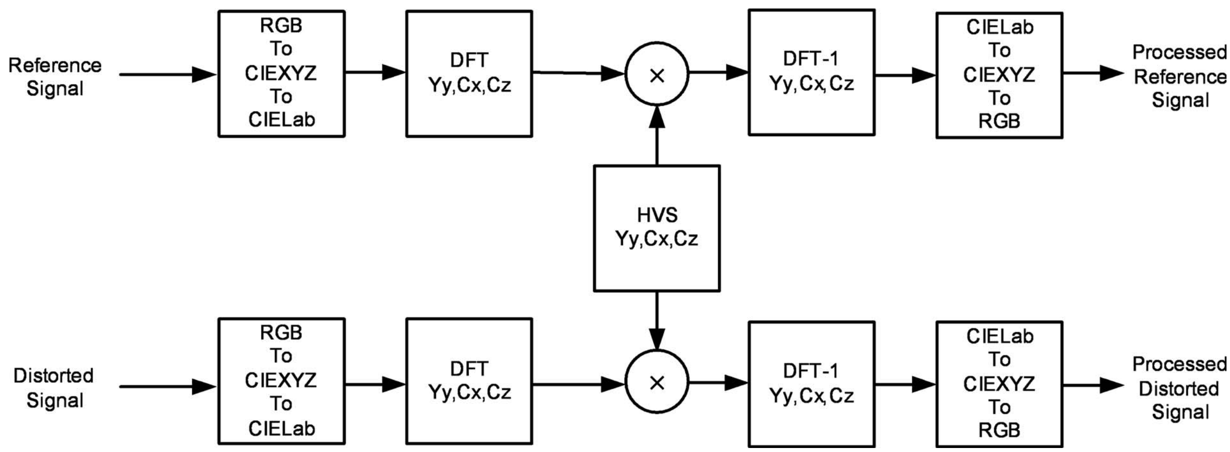

Figure 7. System block diagram for color HVS part in CISM.

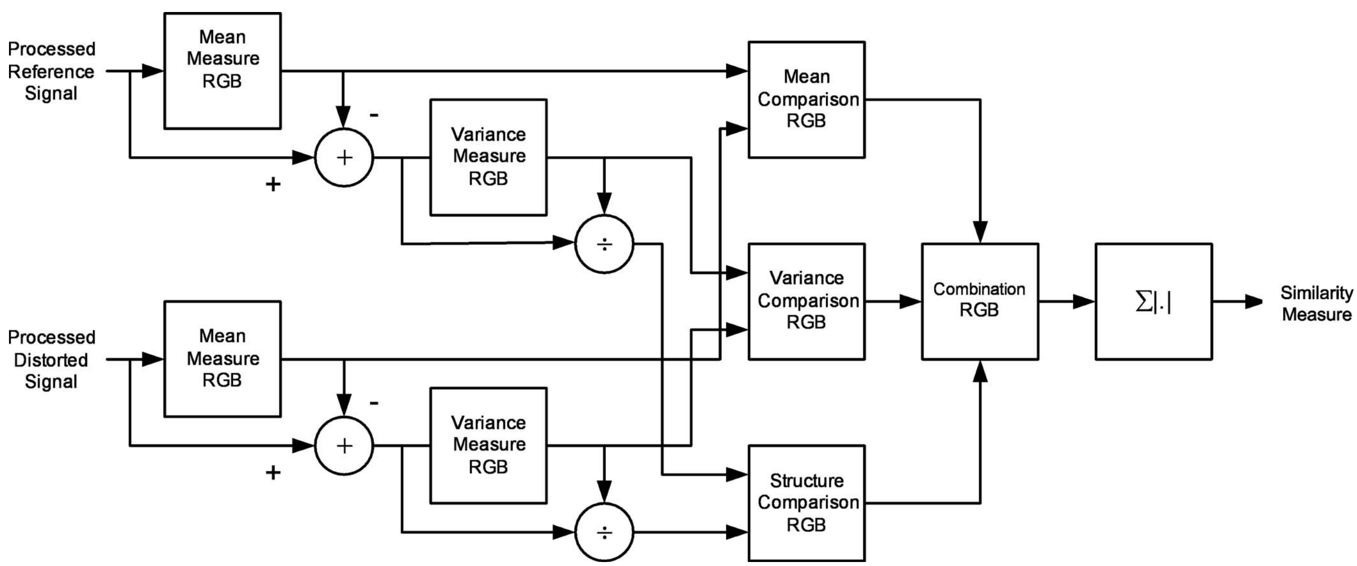

Figure 8. System block diagram for the structural similarity measure part in CISM.

Halftone Statistics: Point Process

We introduce the conventional point process statistics to evaluate the halftone image. The candidates are *pair correlation* and *radially averaged power spectrum density* (*RAPSD*).[11] Pair correlation, the first candidate, is the influence that the point at y has at any x in the spatial annular ring. The pair correlation is a strong indicator of the interpoint relationships for a given pattern. The pair correlation $R(r)$ is known as

$$R(r) = \frac{E\{\phi(R_y(r)) | y \in \phi\}}{E\{\phi(R_y(r))\}}, \tag{10}$$

where y is the point that is influenced by x. ϕ is the sample of point process. Spectral analysis was first applied to stochastic patterns by Ulichney[12] to characterize patterns created via error diffusion. To do so, Ulichney developed the radially averaged power spectra along with a measure of anisotropy. The radially averaged power spectrum is as follows:

$$\hat{P}(f) = \frac{1}{K}\sum_{i=1}^{K} \frac{|\mathrm{DFT}_{2\mathrm{D}}(\phi_i)|^2}{N(\phi_i)}, \tag{11}$$

where $\mathrm{DFT}_{2\mathrm{D}}(\phi)$ represents the two-dimensional, discrete Fourier transform of the sample ϕ, $N(\phi)$ is the total number of pixels in the sample ϕ, and K is the total number of periodic area being averaged to form to estimate. Finally, the RAPSD is defined as follows:

$$P(f_\rho) = \frac{1}{N(R(f_\rho))} \sum_{f \in R(f_\rho)} \hat{P}(f), \tag{12}$$

where $R(f_\rho)$ is the series of annular rings and $N(R(f_\rho))$ is the number of frequency samples in $R(f_\rho)$.

Color Image Similarity Measure

In this section, we introduce the evaluation method, color image similarity measure (CISM), used to evaluate the HED algorithm. The color image similarity measure is largely composed of two blocks. The first one is the color consid-

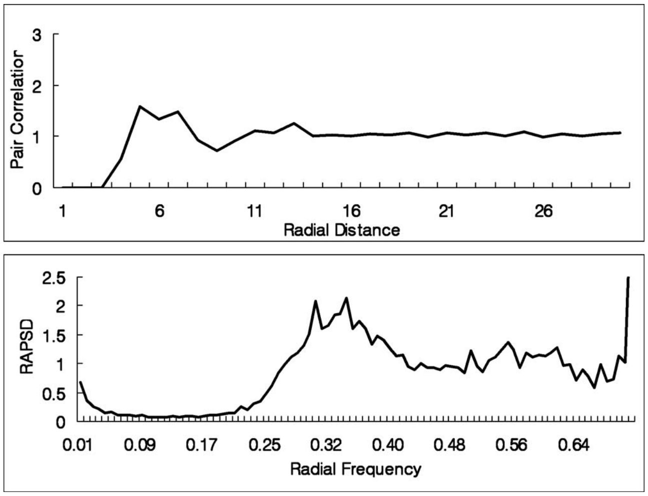

Figure 9. Results of gray level 28 with the Floyd–Steinberg algorithm: Pair correlation/RAPSD.

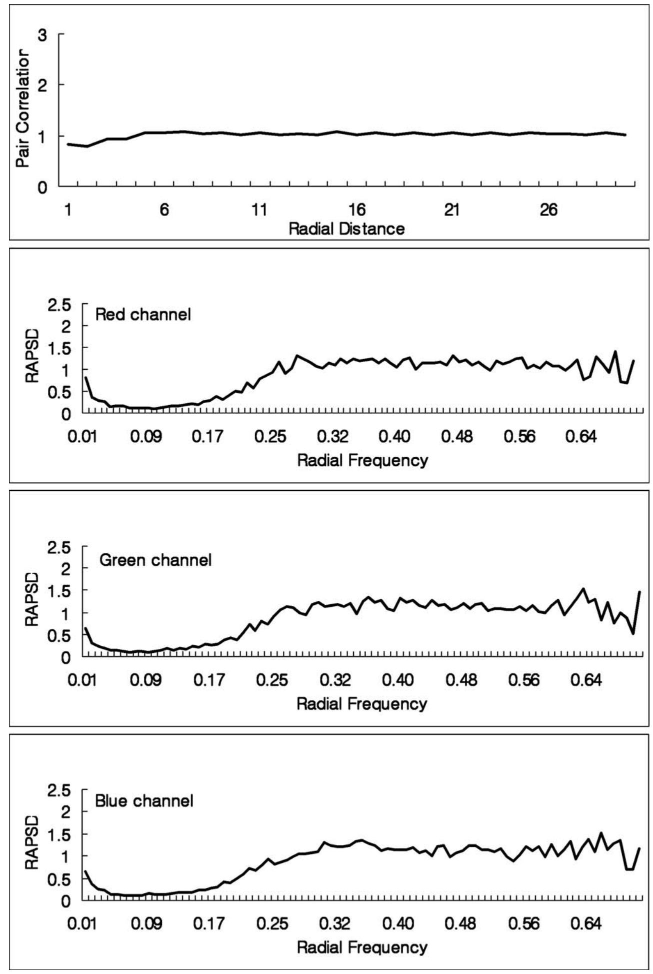

Figure 10. Results of gray level 28 with the hybrid error diffusion algorithm: Pair correlation/RAPSD for each RGB channel.

ering block with the human visual system (HVS) and color image structural similarity calculation block as shown in Figure 6. As introducing the color HVS model, we could consider the interrelation for each color channel in structural similarity measure. A color HVS model takes into account the correlation among color planes. The HVS model is based on a transformation to CIELab color space and exploits the spatial frequency sensitivity variation of the luminance and chrominance channels. Having a model of the HVS allows us to measure the distortion seen by a human viewer.

Color HVS block

The color HVS block is composed of several subblock, color space conversion, discrete Fourier transform, and human visual filters as shown in Figure 7. We carry out the color space conversion to use the human visual frequency response model. The RGB image was transformed to CIEXYZ, and then to CIELab color space. We denote the L, a^*, b^* as the Y_y, C_x, C_z for the convenience of equation, respectively.

As a luminance HVS filter, we use the model that is proposed by Sullivan et al.[13] and Nasanen.[14] The contrast sensitivity of the human viewer to spatial variations in chrominance falls off faster as a function of increasing spatial frequency than does the response to spatial variations in luminance. This HVS chrominance filter is based on the experimental results obtained by Mullen.[15] The details of the HVS model are in Appendix I (available as Supplemental Material on IS&T website, www.imaging.org).

The flow of the color HVS block is as follows. Let $x_{(\mathrm{R,G,B})}(m,n)$ and $y_{(\mathrm{R,G,B})}(m,n)$ denote the continuous tone image and distorted image, respectively. $x_{(Y_y,C_x,C_z)}(m,n)$ and $y_{(Y_y,C_x,C_z)}(m,n)$ are obtained by transforming $x_{(\mathrm{R,G,B})}(m,n)$ and $y_{(\mathrm{R,G,B})}(m,n)$ to the $Y_yC_xC_z$ color space,

$$X_{(Y_y,C_x,C_z)}(k,l) = \mathrm{DFT}(x_{(Y_y,C_x,C_z)}(m,n)), \tag{13}$$

$$Y_{(Y_y,C_x,C_z)}(k,l) = \mathrm{DFT}(y_{(Y_y,C_x,C_z)}(m,n)), \tag{14}$$

$$H_{\mathrm{HVS}}(k,l) = (H_{Y_y}(k,l), H_{C_x}(k,l), H_{C_z}(k,l)), \tag{15}$$

$$P_{X_{(Y_y,C_x,C_z)}}(k,l) = X_{(Y_y,C_x,C_z)}(k,l)H_{\mathrm{HVS}}(k,l), \tag{16}$$

$$P_{Y_{(Y_y,C_x,C_z)}}(k,l) = Y_{(Y_y,C_x,C_z)}(k,l)H_{\mathrm{HVS}}(k,l), \tag{17}$$

$$x'_{(Y_y,C_x,C_z)}(m,n) = \mathrm{DFT}^{-1}(P_{X_{(Y_y,C_x,C_z)}}(k,l)), \tag{18}$$

$$y'_{(Y_y,C_x,C_z)}(m,n) = \mathrm{DFT}^{-1}(P_{Y_{(Y_y,C_x,C_z)}}(k,l)), \tag{19}$$

where DFT is the discrete Fourier transform and DFT^{-1} is the inverse discrete Fourier transform. The HVS filters are applied to the luminance and chrominance components in the spatial frequency domain. Finally, the output of the color HVS part is $x'_{(\mathrm{R,G,B})}(m,n)$ and $y'_{(\mathrm{R,G,B})}(m,n)$, which is transformed to RGB color space, taking HVS into account. This is the input to the structural similarity measure block.

Structural similarity measure block

The system block diagram for the structural similarity (SSIM) measure block in CISM is shown in Figure 8. The

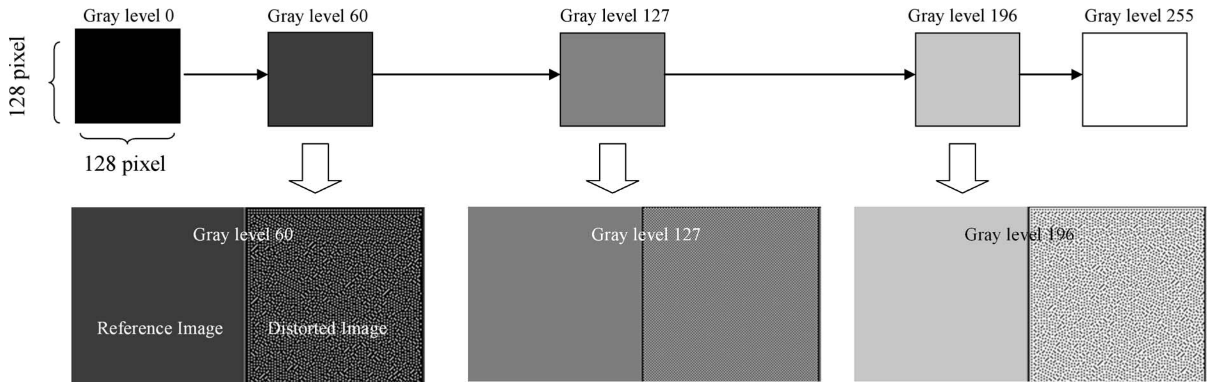

Figure 11. Inputs of the structural similarity measure and the color image similarity measure.

SSIM algorithm is expanded to RGB color. The structural similarity method was proposed by Wang et al.[16,17] The SSIM compares local patterns for pixel intensities that have been normalized for luminance and contrast between a reference image and a distorted image. The MSSIM is the mean structural similarity measure for entire image. The details of the SSIM and MSSIM are in Appendix II (available as Supplemental Material on IS&T website, www.imaging.org). In this paper, we expand the concept of MSSIM to color images. The input of the structural similarity measure part is $x'_{(R,G,B)}(m,n)$ and $y'_{(R,G,B)}(m,n)$, which was already processed with consideration of the HVS. The final output of CISM is the weighted sum of the MSSIM value for each channel in RGB color as shown in

$$\mathrm{CISM}(x,y) = \sum_i w_i \mathrm{MSSIM}(x,y), \tag{20}$$

where w_i is the weight for each channel in RGB color. In this paper, we used the value of $w_i = 1/3$.

Evaluation and Experimental Results

In order to verify the proposed algorithm, we compared the conventional error diffusion algorithm, Floyd–Steinberg error diffusion algorithm,[1] vector color error diffusion,[7] and Shiau–Fan error diffusion[10] with the proposed algorithm.

Results of Halftone Statistics

The results of pair correlation and RAPSD are shown in Figures 9 and 10. The input image resolution is a 128 $\times$ 128 pixel image with a gray level of 28 as shown in Fig. 4. Figure 9 is the result of the Floyd–Steinberg algorithm, and Fig. 10 is the result of hybrid error diffusion. For the result of pair correlation, $R(r)=0$ for $r<3.5$ is a consequence of the inhibition of points within a distance of 3.5 of each other. The more frequent occurrence of halftone result is in the distance of $4.5<r<7.5$ with the condition of $R(r)>1$. There is no area for the case of $R(r)=0$ in Fig. 10. This means that the hybrid error diffusion can offer the chance of occurrence in the RGB mixed model.

For the result of RAPSD, it has a power spectrum that is composed entirely of high frequencies, in the case of the Floyd–Steinberg algorithm in Fig. 9. However, the power spectrum of hybrid error diffusion is extended to the lower frequency area and the high frequency components are suppressed. This means that the density of a dot is increased and spread with a good pattern profile.

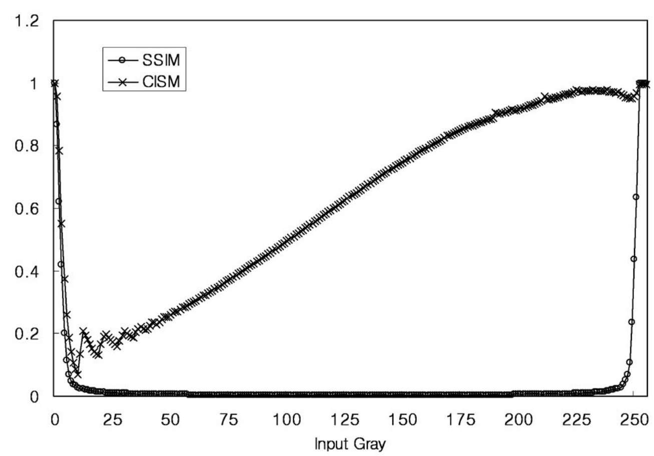

Figure 12. Comparison of the structural similarity measure and the color image similarity measure: Floyd–Steinberg error diffusion (raster scan).

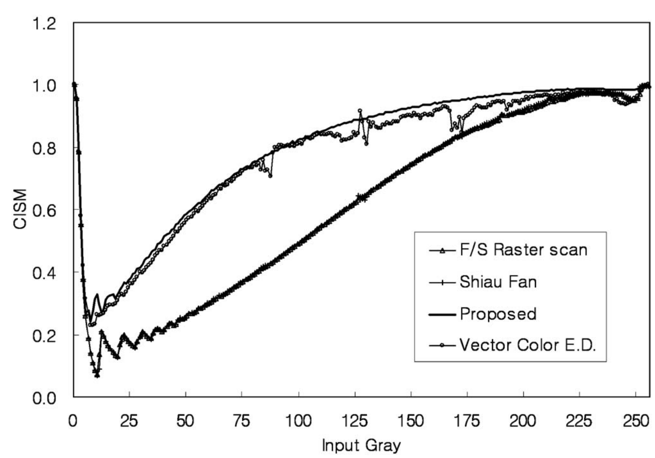

Figure 13. Objective evaluation results: Color image similarity measure.

Results for the Gradation Characteristic

First, we try to show the capability of MSSIM and CISM to assess the halftone image quality. We used the Floyd–Steinberg error diffusion (raster scan) as a test halftone

Table I. Numerical data: Color image similarity measure (CISM).

Input Gray	F/S E.D. Raster Scan	Shiau–Fan E.D.	Proposed HED	Vector Color E.D.
0	1.0000	1.0000	1.0000	1.0000
1	0.9556	0.9556	0.9556	0.9556
2	0.7842	0.7842	0.7842	0.7867
3	0.5526	0.5526	0.5526	0.5779
4	0.3760	0.3760	0.3760	0.4222
5	0.2615	0.2615	0.2718	0.3143
6	0.1886	0.1886	0.2793	0.2661
7	0.1410	0.1410	0.2448	0.2307
8	0.1089	0.1089	0.2751	0.2290
9	0.0863	0.0863	0.3149	0.2324
10	0.0705	0.0701	0.3280	0.2643
11	0.1362	0.0883	0.2964	0.2610
12	0.2079	0.2076	0.2693	0.2654
13	0.1956	0.1956	0.2798	0.2658
14	0.1793	0.1793	0.3135	0.2778
15	0.1654	0.1654	0.3217	0.2902
16	0.1534	0.1534	0.3268	0.2956
17	0.1429	0.1429	0.3303	0.2963
18	0.1338	0.1338	0.3150	0.2969
19	0.1301	0.1269	0.3305	0.3084
20	0.1677	0.1621	0.3421	0.3242
21	0.1908	0.1768	0.3544	0.3302
22	0.1972	0.1969	0.3651	0.3252
23	0.1883	0.1883	0.3619	0.3353
24	0.1800	0.1800	0.3753	0.3509
25	0.1724	0.1724	0.3813	0.3644
26	0.1654	0.1654	0.3933	0.3639
27	0.1599	0.1591	0.3886	0.3733
28	0.1782	0.1734	0.4098	0.3836
29	0.1947	0.1925	0.4162	0.3998
30	0.2076	0.2063	0.4266	0.3994
31	0.2015	0.2015	0.4403	0.4037
32	0.1951	0.1951	0.4449	0.4155
33	0.1890	0.1890	0.4494	0.4232
34	0.1881	0.1849	0.4626	0.4283
35	0.2044	0.2015	0.4685	0.4377
36	0.2166	0.2148	0.4741	0.4529
37	0.2206	0.2211	0.4898	0.4608
38	0.2155	0.2155	0.4954	0.4701
39	0.2103	0.2099	0.4990	0.4704
40	0.2150	0.2112	0.5138	0.4835
41	0.2269	0.2275	0.5202	0.4876
42	0.2361	0.2371	0.5257	0.4983
43	0.2350	0.2357	0.5348	0.5041
44	0.2304	0.2304	0.5397	0.5160

Table I. (*Continued.*)

Input Gray	F/S E.D. Raster Scan	Shiau–Fan E.D.	Proposed HED	Vector Color E.D.
45	0.2348	0.2319	0.5523	0.5264
46	0.2459	0.2455	0.5540	0.5297
47	0.2516	0.2535	0.5645	0.5396
48	0.2520	0.2516	0.5714	0.5501
49	0.2527	0.2487	0.5815	0.5567
50	0.2593	0.2594	0.5873	0.5658
51	0.2668	0.2682	0.5938	0.5725
52	0.2689	0.2694	0.5994	0.5774
53	0.2700	0.2667	0.6072	0.5850
54	0.2759	0.2765	0.6147	0.5956
55	0.2829	0.2846	0.6214	0.5936
56	0.2848	0.2847	0.6223	0.6044
57	0.2869	0.2870	0.6304	0.6112
58	0.2936	0.2952	0.6393	0.6215
59	0.2992	0.3012	0.6459	0.6268
60	0.3005	0.3005	0.6531	0.6405
61	0.3062	0.3084	0.6607	0.6345
62	0.3121	0.3155	0.6627	0.6458
63	0.3146	0.3163	0.6686	0.6475
64	0.3220	0.3265	0.6780	0.6646
65	0.3231	0.3240	0.6805	0.6640
66	0.3286	0.3274	0.6794	0.6772
67	0.3327	0.3319	0.6911	0.6753
68	0.3371	0.3393	0.6970	0.6796
69	0.3423	0.3418	0.7011	0.6922
70	0.3465	0.3468	0.7049	0.6892
71	0.3518	0.3527	0.7124	0.6953
72	0.3559	0.3554	0.7172	0.7046
73	0.3613	0.3618	0.7217	0.7085
74	0.3661	0.3663	0.7300	0.7145
75	0.3703	0.3699	0.7317	0.7230
76	0.3762	0.3764	0.7370	0.7297
77	0.3800	0.3805	0.7352	0.7341
78	0.3853	0.3866	0.7420	0.7338
79	0.3903	0.3914	0.7495	0.7333
80	0.3948	0.3961	0.7538	0.7430
81	0.4001	0.4018	0.7533	0.7423
82	0.4043	0.4074	0.7612	0.7474
83	0.4097	0.4143	0.7646	0.7281
84	0.4146	0.4191	0.7675	0.7570
85	0.4199	0.4230	0.7739	0.7248
86	0.4219	0.4213	0.7736	0.7264
87	0.4290	0.4275	0.7817	0.7065
88	0.4333	0.4331	0.7842	0.7808
89	0.4390	0.4379	0.7883	0.7991

Table I. (*Continued.*)

Input Gray	F/S E.D. Raster Scan	Shiau–Fan E.D.	Proposed HED	Vector Color E.D.
90	0.4437	0.4430	0.7902	0.7993
91	0.4490	0.4486	0.7945	0.8058
92	0.4538	0.4531	0.7995	0.8049
93	0.4591	0.4586	0.7993	0.8039
94	0.4638	0.4631	0.8047	0.8022
95	0.4694	0.4690	0.8071	0.8051
96	0.4743	0.4734	0.8132	0.8034
97	0.4795	0.4789	0.8179	0.8061
98	0.4847	0.4840	0.8142	0.8030
99	0.4898	0.4890	0.8236	0.8107
100	0.4952	0.4948	0.8257	0.8131
101	0.4999	0.4996	0.8257	0.8099
102	0.5055	0.5052	0.8305	0.8227
103	0.5106	0.5088	0.8342	0.8284
104	0.5157	0.5152	0.8346	0.8295
105	0.5213	0.5207	0.8379	0.8275
106	0.5262	0.5256	0.8417	0.8309
107	0.5315	0.5312	0.8460	0.8361
108	0.5369	0.5363	0.8489	0.8406
109	0.5417	0.5412	0.8477	0.8444
110	0.5472	0.5467	0.8512	0.8397
111	0.5527	0.5521	0.8534	0.8407
112	0.5577	0.5569	0.8557	0.8400
113	0.5628	0.5622	0.8601	0.8449
114	0.5686	0.5678	0.8627	0.8441
115	0.5734	0.5726	0.8633	0.8369
116	0.5783	0.5778	0.8665	0.8336
117	0.5843	0.5836	0.8701	0.8411
118	0.5891	0.5884	0.8713	0.8350
119	0.5939	0.5934	0.8731	0.8203
120	0.5989	0.5982	0.8762	0.8230
121	0.6043	0.6035	0.8790	0.8226
122	0.6092	0.6085	0.8804	0.8277
123	0.6143	0.6137	0.8826	0.8299
124	0.6194	0.6187	0.8873	0.8472
125	0.6251	0.6236	0.8869	0.8352
126	0.6306	0.6434	0.8894	0.8440
127	0.6368	0.6395	0.8894	0.9160
128	0.6401	0.6357	0.8909	0.8827
129	0.6447	0.6318	0.8917	0.8286
130	0.6494	0.6486	0.8925	0.8077
131	0.6548	0.6539	0.8982	0.8820
132	0.6603	0.6590	0.8989	0.8629
133	0.6656	0.6645	0.8986	0.8762
134	0.6705	0.6696	0.9034	0.8641

Table I. (*Continued.*)

Input Gray	F/S E.D. Raster Scan	Shiau–Fan E.D.	Proposed HED	Vector Color E.D.
135	0.6759	0.6746	0.9044	0.8604
136	0.6810	0.6795	0.9045	0.8611
137	0.6859	0.6848	0.9066	0.8692
138	0.6911	0.6893	0.9109	0.8713
139	0.6959	0.6945	0.9112	0.8768
140	0.7009	0.6996	0.9126	0.8751
141	0.7059	0.7047	0.9131	0.8752
142	0.7105	0.7093	0.9147	0.8802
143	0.7151	0.7138	0.9158	0.8828
144	0.7200	0.7186	0.9188	0.8798
145	0.7245	0.7231	0.9209	0.8933
146	0.7293	0.7279	0.9228	0.8984
147	0.7338	0.7326	0.9216	0.8969
148	0.7382	0.7370	0.9247	0.9007
149	0.7429	0.7418	0.9246	0.9018
150	0.7473	0.7465	0.9288	0.8984
151	0.7521	0.7510	0.9283	0.9070
152	0.7568	0.7571	0.9299	0.9031
153	0.7612	0.7607	0.9307	0.9020
154	0.7654	0.7649	0.9312	0.8913
155	0.7700	0.7695	0.9365	0.9016
156	0.7747	0.7739	0.9354	0.9045
157	0.7786	0.7781	0.9349	0.9021
158	0.7832	0.7822	0.9357	0.9049
159	0.7873	0.7868	0.9404	0.9027
160	0.7913	0.7911	0.9415	0.9157
161	0.7956	0.7953	0.9391	0.9194
162	0.8000	0.7992	0.9431	0.9201
163	0.8038	0.8040	0.9431	0.9225
164	0.8077	0.8077	0.9446	0.9274
165	0.8119	0.8114	0.9447	0.9292
166	0.8159	0.8157	0.9460	0.9268
167	0.8200	0.8192	0.9454	0.9168
168	0.8248	0.8242	0.9486	0.8530
169	0.8332	0.8321	0.9489	0.8756
170	0.8336	0.8312	0.9499	0.8611
171	0.8360	0.8328	0.9502	0.8943
172	0.8393	0.8348	0.9540	0.8480
173	0.8429	0.8399	0.9526	0.8902
174	0.8461	0.8440	0.9542	0.8993
175	0.8498	0.8482	0.9557	0.9003
176	0.8531	0.8514	0.9541	0.9073
177	0.8564	0.8551	0.9568	0.9158
178	0.8596	0.8588	0.9570	0.9254
179	0.8622	0.8625	0.9595	0.9313

Table I. (*Continued.*)

Input Gray	F/S E.D. Raster Scan	Shiau–Fan E.D.	Proposed HED	Vector Color E.D.
180	0.8649	0.8662	0.9587	0.9290
181	0.8675	0.8699	0.9594	0.9261
182	0.8702	0.8731	0.9623	0.9246
183	0.8726	0.8764	0.9609	0.9273
184	0.8754	0.8791	0.9630	0.9370
185	0.8782	0.8827	0.9634	0.9316
186	0.8800	0.8860	0.9643	0.9432
187	0.8838	0.8888	0.9655	0.9429
188	0.8847	0.8920	0.9658	0.9475
189	0.8865	0.8974	0.9679	0.9477
190	0.9059	0.9015	0.9689	0.9424
191	0.9025	0.9034	0.9709	0.9466
192	0.9006	0.9030	0.9708	0.9201
193	0.9035	0.9051	0.9719	0.9375
194	0.9043	0.9075	0.9718	0.9325
195	0.9073	0.9099	0.9737	0.9457
196	0.9105	0.9117	0.9727	0.9461
197	0.9145	0.9159	0.9750	0.9470
198	0.9132	0.9168	0.9738	0.9409
199	0.9132	0.9193	0.9760	0.9496
200	0.9166	0.9220	0.9765	0.9498
201	0.9182	0.9245	0.9772	0.9595
202	0.9202	0.9275	0.9769	0.9547
203	0.9237	0.9303	0.9788	0.9594
204	0.9263	0.9333	0.9785	0.9589
205	0.9279	0.9352	0.9798	0.9637
206	0.9309	0.9381	0.9799	0.9637
207	0.9327	0.9404	0.9799	0.9620
208	0.9359	0.9427	0.9809	0.9630
209	0.9386	0.9458	0.9812	0.9664
210	0.9425	0.9483	0.9822	0.9655
211	0.9574	0.9569	0.9817	0.9628
212	0.9460	0.9528	0.9824	0.9644
213	0.9478	0.9536	0.9823	0.9612
214	0.9486	0.9556	0.9836	0.9662
215	0.9520	0.9583	0.9829	0.9665
216	0.9533	0.9605	0.9841	0.9633
217	0.9547	0.9616	0.9845	0.9728
218	0.9561	0.9618	0.9853	0.9676
219	0.9595	0.9632	0.9861	0.9703
220	0.9627	0.9651	0.9851	0.9718
221	0.9641	0.9664	0.9856	0.9729
222	0.9658	0.9674	0.9855	0.9710
223	0.9686	0.9671	0.9860	0.9737
224	0.9698	0.9679	0.9865	0.9743

Table I. (*Continued.*)

Input Gray	F/S E.D. Raster Scan	Shiau–Fan E.D.	Proposed HED	Vector Color E.D.
225	0.9785	0.9738	0.9861	0.9764
226	0.9732	0.9700	0.9863	0.9751
227	0.9726	0.9705	0.9861	0.9775
228	0.9754	0.9704	0.9863	0.9754
229	0.9737	0.9732	0.9867	0.9783
230	0.9739	0.9744	0.9866	0.9758
231	0.9744	0.9765	0.9860	0.9760
232	0.9777	0.9789	0.9863	0.9744
233	0.9746	0.9784	0.9860	0.9713
234	0.9749	0.9775	0.9862	0.9731
235	0.9752	0.9742	0.9859	0.9682
236	0.9756	0.9745	0.9850	0.9669
237	0.9757	0.9757	0.9855	0.9696
238	0.9772	0.9748	0.9841	0.9672
239	0.9727	0.9718	0.9855	0.9622
240	0.9714	0.9736	0.9836	0.9487
241	0.9720	0.9710	0.9843	0.9528
242	0.9689	0.9692	0.9838	0.9414
243	0.9711	0.9733	0.9838	0.9394
244	0.9630	0.9640	0.9834	0.9379
245	0.9596	0.9622	0.9831	0.9370
246	0.9553	0.9599	0.9836	0.9379
247	0.9529	0.9560	0.9825	0.9432
248	0.9512	0.9520	0.9838	0.9505
249	0.9508	0.9517	0.9856	0.9578
250	0.9555	0.9561	0.9870	0.9644
251	0.9694	0.9957	0.9896	0.9794
252	0.9964	0.9957	0.9923	0.9813
253	0.9964	0.9957	0.9957	0.9918
254	0.9964	0.9957	0.9957	0.9976
255	0.9964	0.9956	0.9956	1.0000

algorithm. The input image (128×128 pixels) is the constant valued continuous tone image having 0 to 255 gray level, and its corresponding halftone image as shown in Figure 11. The MSSIM and CISM take the value between 0 and 1. When there is no difference between reference image and halftone image, the value is 1. The MSSIM was applied to assess the image quality, such as a jpeg image, noise added image, video source etc.[16,17] From Fig. 12, we can see that the MSSIM must be modified for assessing the halftone visibility. The MSSIM value is close to 0 throughout the gray level besides the high and low gray area. But in the result of CISM, the luminance distortion is mainly shown in the low gray area. The contrast distortion of the halftone image is mainly shown in the high gray area. Although the Gaussian weight (11×11, $\sigma = 1.5$) is applied to the image in the spatial domain, the MSSIM values do not fully comprise the

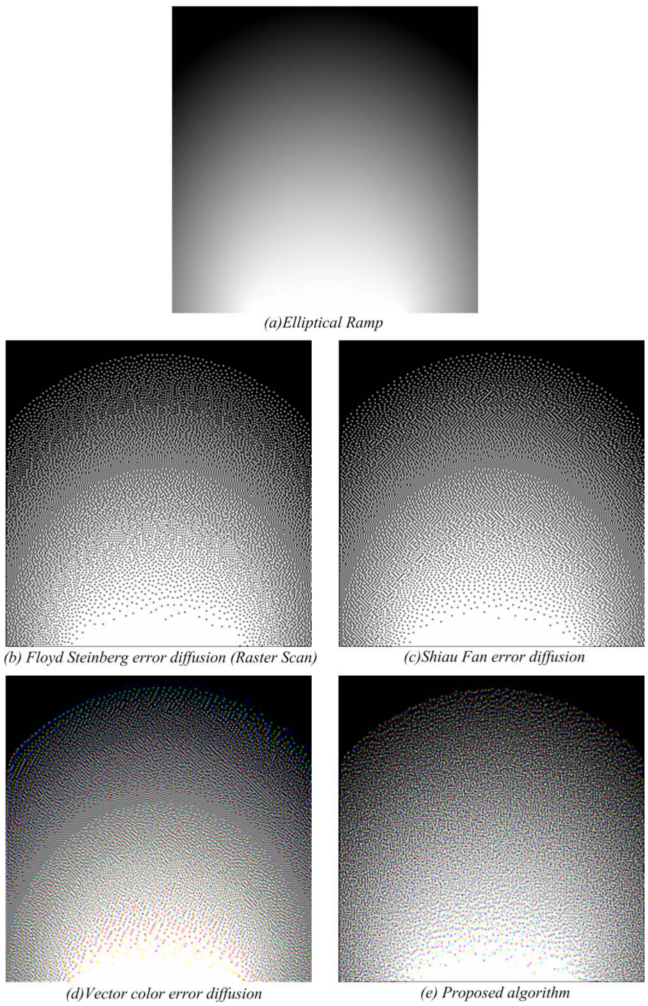

Figure 14. Results of the "elliptical ramp."

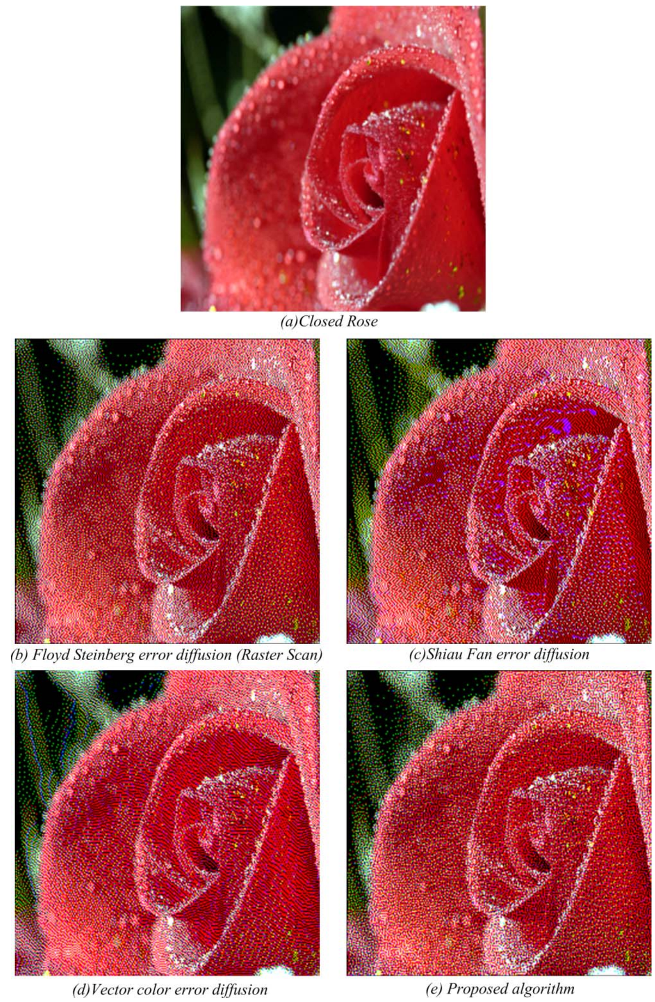

Figure 15. Results of the "closed rose."

concept of the HVS. The color HVS filters contribute to detecting the disturbance of gradation and color correlation of the RGB channel.

In Figure 13, we try to show the visibility characteristics throughout the gray level of various kinds of halftone methods: Floyd–Steinberg error diffusion (raster scan), Shiau–Fan error diffusion, vector color error diffusion, and proposed algorithm. In the cases of conventional error diffusion, the CISM values are lower than that of the proposed algorithm throughout the gray level of 0–255. Especially, the discontinuity of the gradation characteristic is shown in the case of the vector color error diffusion. From the results, the visibility characteristic of HED is outstanding compared to that of the conventional halftone method. The numerical data of CISM is given in Table I.

Results for Natural Images

We compare the results of Floyd–Steinberg error diffusion (raster scan), Shiau–Fan error diffusion, vector color error diffusion, and the proposed algorithm with the source of the "elliptical ramp" image in Figure 14 and the "closed rose" image in Figure 15. The size of source images is 256×256 pixels. In Figs. 14(b)–14(d), false textures are prominent in the middle of elliptical ramp gradation. But as shown in Fig. 14(e), there is no structural pattern caused by the error diffusion in the case of the proposed algorithm. In addition, the proposed algorithm does not suffer from the directional artifacts, such as diagonal worms, which appear in the elliptical ramp edge and highlight area. The gradation of color rendition is also better for the proposed algorithm. The white dots in Figs. 14(b) and 14(c) are replaced by the mixture of red, green, and blue, which is less visible. The numerical data of CISM are given in Table II.

Table II. Numerical data for natural images: Color image similarity measure (CISM).

	F/S E.D. Raster Scan	Shiau–Fan E.D.	Vector Color E.D.	Proposed HED
Elliptical ramp	0.69	0.69	0.87	0.90
Closed rose	0.74	0.61	0.69	0.75

CONCLUSION

In this paper, we proposed a new error diffusion algorithm. The proposed algorithm is very simple, easy to implement, and can reduce the structure artifacts while keeping the advantages of the error diffusion. We use the concept of perturbing error filter weight using the mask, which is selected with a pseudorandom number. The results of the proposed method and conventional error diffusion were compared to the natural image. In addition, the proposed algorithm was evaluated with the objective assessment tools, halftone statistics, and CISM. We improved the gray expression using the mask and pseudorandom number. The color visibility was also improved by using the mixed error diffusion weight method. The proposed algorithm has good performance for improving the gradation characteristics and reducing the structural pattern induced by conventional error diffusion. For future work, we will try to investigate the possibility of adaptation to the flat panel display.

REFERENCES

[1] R. W. Floyd and L. Steinberg, "An adaptive algorithm for spatial gray scale", Proc. SID **17**, 75 (1976).

[2] J. F. Jarvis, C. N. Judice, and W. H. Ninke, "A survey of techniques for the display of continuous tone pictures on bilevel displays", Comput. Graph. Image Process. **5**, 13 (1976).

[3] N. Damera-Venkata and B. L. Evans, "Adaptive threshold modulation for error diffusion halftoning", IEEE Trans. Image Process. **10**, 104 (2001).

[4] P. Li and J. P. Allebach, "Tone dependent error diffusion", IEEE Trans. Image Process. **13**, 201 (2004).

[5] R. Eschbach, "Reduction of artifacts in error diffusion by means of input dependent weights", J. Electron. Imaging **2**, 352 (1993).

[6] V. Monga and B. L. Evans, "Tone dependent color error diffusion", *Proc. IEEE Int. Conf. on Acoustics, Speech, and Signal Proc.* (IEEE, Piscataway, NJ, 2004) Vol. 3, p. 101.

[7] N. Damera-Venkata and B. L. Evans, "Design and analysis of vector color error diffusion halftoning systems", IEEE Trans. Image Process. **10**, 1552 (2001).

[8] J. H. Lee, "Plasma display apparatus and image processing method thereof", US Patent Application, 0,253,782A1 (2005).

[9] D. J. Lieberman and J. P. Allebach, "Model based direct binary search halftone optimization with a dual interpretation", *Proceedings of the IEEE Int. Conf. on Image Proc.* (IEEE, Piscataway, NJ, 1998) Vol. 2, p. 44.

[10] J. N. Shiau and Z. Fan, "Set of easily implementable coefficients in error diffusion with reduced worm artifacts", Proc. SPIE **2658**, 222 (1996).

[11] D. L. Lau and G. R. Arce, *Modern Digital Halftoning* (Marcel Dekker, New York, 2001), pp. 27–45.

[12] R. Ulichney, *Digital Halftoning* (MIT Press, Cambridge, MA, 1987).

[13] J. Sullivan, L. Ray, and R. Miller, "Design of minimum visual modulation halftone patterns", IEEE Trans. Syst. Man Cybern. **21**, 33 (1991).

[14] R. Nasanen, "Visibility of halftone dot textures", IEEE Trans. Syst. Man Cybern. **14**, 920 (1984).

[15] K. T. Mullen, "The contrast sensitivity of human color vision to red-green and blue-yellow chromatic gratings", J. Physiol. (London) **359**, 381 (1985).

[16] Z. Wang, A. C. Bovik, and E. P. Simoncelli, "Structural Approaches to Image Quality Assessment", in *Handbook of Image and Video Processing*, 2nd ed. (Academic Press, New York, 2005), Chapter 8.3.

[17] Z. Wang, A. C. Bovik, H. R. Sheikh, and E. P. Simoncelli, "Image quality assessment: From error visibility to structural similarity", IEEE Trans. Image Process. **13**, 600 (2004).